Infrared dielectric function of *p*-type $Ge_{0.98}Sn_{0.02}$ alloys

Vijay R. D'Costa,[1] John Tolle,[2] Junqi Xie,[2] John Kouvetakis,[2] and José Menéndez[1]
[1]*Department of Physics and Astronomy, Arizona State University, Tempe, Arizona 85287-1504, USA*
[2]*Department of Chemistry and Biochemistry, Arizona State University, Tempe, Arizona 85287-1604, USA*
(Received 21 April 2009; revised manuscript received 13 July 2009; published 25 September 2009)

The dielectric function of heavily doped *p*-type $Ge_{0.98}Sn_{0.02}$ alloys was determined using infrared spectroscopic ellipsometry. The free holes contribute a Drude-like term to the dielectric response, from which the resistivity and carrier relaxation time can be determined. The transport parameters extracted from such optical experiments are similar to those found for pure Ge with comparable doping levels. Optical transitions between the split-off, light-hole, and heavy-hole bands contribute a second term to the dielectric function. The overall line shape of the dielectric function corresponding to these transitions shows differences between $Ge_{0.98}Sn_{0.02}$ and pure Ge. These differences may provide important clues to the valence-band electronic structure of $Ge_{1-y}Sn_y$ alloys.

DOI: 10.1103/PhysRevB.80.125209 PACS number(s): 78.20.Ci, 73.50.−h

I. INTRODUCTION

$Ge_{1-y}Sn_y$ alloys possess an intriguing potential for infrared optoelectronics.[1] Prototype photoconductor devices have already been demonstrated.[2] Since the lowest direct gap of the alloy is lower than that of Ge,[3] the presence of even a small amount of Sn extends the infrared performance of $Ge_{1-y}Sn_y$-based optoelectronic devices to the entire range of transmission windows for telecom applications. Furthermore, a linear band-structure interpolation between Ge and α-Sn—supported by early theoretical work[4,5]—leads to a direct-band gap alloy for $y>0.2$, raising the possibility of laser applications. Recent experimental work[6–8] suggests that the band gap becomes direct for even smaller Sn concentrations. The latest theoretical calculations confirm this conclusion and place the indirect to direct-gap crossover at 6.5% Sn.[9]

Critical for the realization of the infrared device potential of $Ge_{1-y}Sn_y$ alloys is the development of doping protocols and the study of the transport properties of doped materials. In this paper, we describe the growth and characterization of highly doped *p*-type $Ge_{0.98}Sn_{0.02}$ layers on Si. Earlier work by our group has addressed *n*-type $Ge_{1-y}Sn_y$ alloys and presented preliminary results for *p* doping.[10,11]

The $k\cdot p$ method[12] can be used to describe the valence-band structure of $Ge_{1-y}Sn_y$ alloys in the spirit of the virtual-crystal approximation.[13] Within this framework, the lowering of the direct gap E_0 as a function of the Sn concentration does not affect the value of the heavy-hole mass, so that for $y=0.02$ the main effect of alloying on hole mobilities is the additional relaxation induced by alloy scattering. In $Si_{1-x}Ge_x$ alloys with $x\sim0.05$ or $x\sim0.95$, alloy scattering reduces the phonon-limited hole mobility by as much as 50%.[14] Calculations of alloy scattering for tensile-strained $Ge_{1-y}Sn_y$ were performed by Sau and Cohen.[13] No results have been reported for relaxed $Ge_{1-y}Sn_y$ alloys, but the much larger bowing in the compositional dependence of their optical transitions relative to $Si_{1-x}Ge_x$ alloys[6] suggests that the effect of alloy scattering on the hole mobility in $Ge_{1-y}Sn_y$ alloys should be even more pronounced. However, for carrier concentrations $p>10^{18}$ cm^{-3} ionic impurity scattering becomes dominant and, therefore, the transport properties of $Ge_{1-y}Sn_y$ alloys at these hole concentrations are expected to be very similar to those of pure Ge. On the other hand, Alberi *et al.* used a band anticrossing model beyond the virtual-crystal approximation to explain the compositional dependence of the direct-band gap in $Ge_{1-y}Sn_y$ alloys.[8] These authors modeled the alloy by introducing an impuritylike level associated with the Sn 5*p* states. This level is located below the Ge 4*p* states and causes an increase in the heavy-hole mass by level repulsion. Thus, they predicted a reduced hole mobility for all doping concentrations.

For an experimental test of the above predictions, we use infrared spectroscopic ellipsometry. This technique measures the complex dielectric function and makes it possible to determine the material's transport properties from its Drude-like free-carrier response. The contactless nature of spectroscopic ellipsometry is useful whenever electrical measurements are very challenging—such as the present study of thin films grown on conductive substrates. Moreover, the technique makes it possible to determine doping profiles,[15,16] a feature of considerable value for the study of device structures. Spectroscopic ellipsometry is particularly suitable for the study of *p*-doped materials because intervalence-band optical transitions contribute to the infrared dielectric function. Thus, the validity of electronic structure models can be tested not only indirectly via the impact on transport properties but also by spectroscopically probing into the valence-band states. The spectroscopic signature of intervalence-band absorption is a series of relatively broad bands that appear as shoulders superposed to the dominant Drude-like free-carrier response in the imaginary part of the dielectric function. These bands correspond to optical transitions between the split-off (SO), light-hole (LH), and heavy-hole (HH) bands and allow a simple distinction between *p*-type and *n*-type group-IV materials on the basis of the shape of the dielectric function.

The infrared absorption of *p*-type Ge has been studied in detail since the early 1950s,[17–20] but these studies were limited to lightly doped samples. A systematic study of the infrared dielectric response of heavily doped group-IV semiconductors has yet to be reported. Our initial studies on doped GeSn alloys show excellent agreement between pa-

rameters obtained from electrical measurements and ellipsometry.[11] Previous infrared ellipsometry studies on *p*-type group-IV were carried out by Humlíček,[21] Humlíček and Křapek,[22] and Chen *et al.*[23] Humlícek and Křapek studied the infrared response of *p*-type Si, SiGe, and Ge. The dielectric function was interpreted in terms of free-carrier response and intervalence-band transitions. A theoretical study using the $k \cdot p$ method was used to compute the intervalence-band contribution to the dielectric function of Si. Chen *et al.* used infrared ellipsometry to determine the boron concentration and Ge concentration in heavily doped Si-rich $Si_{1-x}Ge_x$ alloys. However, they did not account for the intervalence absorption in their analysis.

Our studies confirm that doping of $Ge_{1-y}Sn_y$ alloys at the high levels needed for device application is possible. We find that the transport properties of these heavily doped alloys are very similar to those of pure Ge doped at the same level. However, we cannot rule out the validity of the band anticrossing model because no quantitative effective-mass predictions have been made based on this model. Moreover, we find distinct differences between intervalence-band absorption bands in pure Ge and $Ge_{1-y}Sn_y$ alloys that might be due to the distortion of the valence-band dispersion relations predicted by Alberi *et al.*[8]

II. GROWTH DETAILS AND STRUCTURAL CHARACTERIZATION

The growth of *p*-type GeSn samples was performed via UHV CVD on resistive (ρ=3000–4000 Ω cm) and conductive (ρ=0.01–0.02 Ω cm, *p*-type) Si(100) substrates via *in situ* reactions of conventional B_2H_6 and appropriate concentrations of Ge_2H_6/SnD_4 diluted in high-purity H_2. The dopant level in the material was readily controlled in the range of 10^{18}–10^{19} atoms/cm^3 by adjusting the B_2H_6:Ge_2H_6 ratio in the gas mixture between 1:3000 and 1:100, respectively. The depositions were conducted at 350 °C, producing highly uniform $Ge_{0.98}Sn_{0.02}$ layers with atomically flat surfaces (rms roughness of 1–1.5 nm for 80×80 μm^2 areas) and an average thickness approaching 1 μm. The growth rate of these samples was found to be ~15 nm/min and is slightly higher than that of ~10 nm/min obtained for intrinsic alloys with the same $Ge_{0.98}Sn_{0.02}$ composition and similar thicknesses. High-resolution x-ray diffraction (XRD) analyses indicated that the as-deposited *p*-doped films possessed a residual compressive strain of 0.25%. After heating the samples at 850 °C for 2 s under a flow of N_2 using rapid thermal annealing (RTA) conditions, the samples develop a small tensile strain of about 0.15%. The XRD data showed that the RTA processed B-doped $Ge_{0.98}Sn_{0.02}$ films exhibited superior in-plane crystallographic alignment compared to the intrinsic counterparts, as evidenced by the substantially lower value of the full width at half maximum for the (004) rocking curves (0.17° vs 0.22°) and subsequent cross-section transmission electron microscopy (XTEM) observations. This improvement in crystallinity may be attributed to the smaller B atoms in the tetrahedral structure providing local strain compensation induced by the presence of the larger Sn atoms in the Ge-like lattice. To further explore this possibility, we conducted precise measurements of the lattice dimensions of highly concentrated samples with B contents of 7–8 $\times 10^{19}$/cm^3. The results indicated that the average unit-cell parameters are slightly lower by 0.07% compared to that of the corresponding intrinsic material (background carrier concentration of 10^{15}/cm^3 *p*-type), consistent with the notion that the B atom counterbalancing the bond strain distribution introduced by Sn. Complementary XTEM observations confirmed the smooth surface morphology obtained by atomic force microscopy and revealed a rather featureless contrast throughout most of the bulk layer above the interface in bright field images. Nevertheless, occasional threading defects originating at the interface and penetrating through the entire film thickness were also observed within the field of view of the TEM micrographs, particularly, in lower magnifications. High-resolution images showed an array of edge-type dislocations confined to the interface plane providing strain relief between the two highly mismatched materials. Secondary ion mass spectroscopy (SIMS) analysis yielded perfectly homogenous elemental distributions of the host atoms Ge, Sn, and the B dopant as shown in Fig. 1. The B content in all cases was quantified using a Ge wafer implanted with ^{11}B as a standard and the results typically indicated a close agreement with the carrier concentration obtained by Hall measurements and spectroscopic ellipsometry. In particular, for the SIMS data shown in Fig. 1, the B content is found to be nearly identical to that obtained by Hall (4.6×10^{19} cm^{-3} vs 4.7×10^{19} cm^{-3}) implying that the entire B content in this film is electrically active.

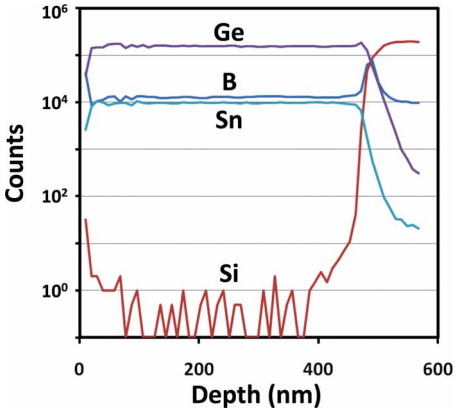

FIG. 1. (Color online) SIMS elemental profiles of Si, Ge, Sn, and B for a $Ge_{0.98}Sn_{0.02}$ sample doped with B atoms at a level of $\sim 5 \times 10^{19}$/cm^3.

III. OPTICAL PROPERTIES

A. Ellipsometric measurements and data processing

Spectroscopic ellipsometry measurements were carried out at room temperature using an infrared variable angle spectroscopic ellipsometer manufactured by J. A. Woollam Co. The infrared variable angle spectroscopic ellipsometer system is based on a Fourier-transform infrared spectrometer and covers the 0.04–0.62 eV range. Two reference *p*-doped Ge substrates were investigated along with the alloys. The

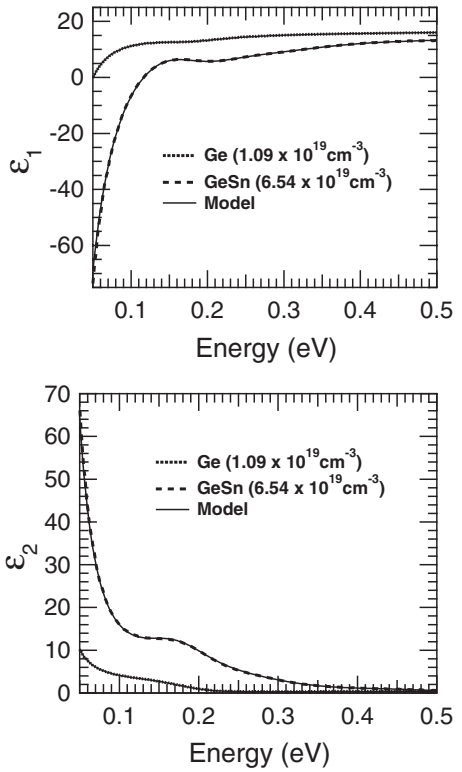

FIG. 2. Infrared real (a) and imaginary (b) parts of parametric and nonparametric (point-by-point fit) dielectric function for a heavily doped *p*-type $Ge_{0.98}Sn_{0.02}$ alloy and *p*-doped Ge.

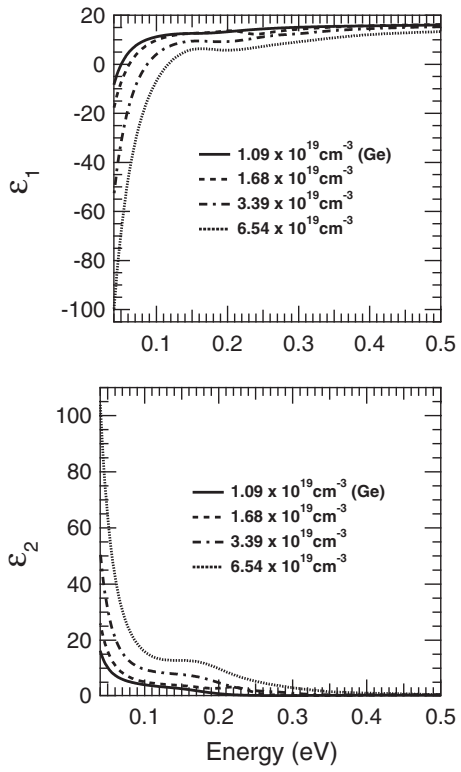

FIG. 3. Infrared real (a) and imaginary (b) parts of the dielectric function of various heavily doped *p*-type $Ge_{0.98}Sn_{0.02}$ alloys and a *p*-doped Ge.

measurements were performed at three angles of incidence (65°, 70°, and 75°). The $Ge_{0.98}Sn_{0.02}$ films were modeled as a three layer system consisting of a Si substrate, a film layer, and a surface layer. The dielectric function of Si substrate with a resistivity of 0.01–0.02 Ω cm was measured separately and used in tabulated form. The surface layer was modeled as a thin film consisting of 50% GeSn and 50% voids in the Bruggeman approximation.[24] The dielectric function of the $Ge_{0.98}Sn_{0.02}$ alloy was described using an optical dispersion model given by

$$\varepsilon(E) = C + \frac{-\hbar^2}{\varepsilon_0\rho(\tau E^2 + i\hbar E)} + \sum_{k=1}^{m}(\varepsilon_1^k + i\varepsilon_2^k) + \frac{A_{pole}}{(E_{pole}^2 - E^2)}, \tag{1}$$

where $\varepsilon_2^k = A(e^{-((E-E^k)/\sigma^k)^2} - e^{-((E+E^k)/\sigma^k)^2})$. C is a constant that is taken as an adjustable parameter. The second term is related to the Drude line shape that describes the free hole behavior in the valence band.[16] Here ρ is the electrical resistivity and τ is the carrier relaxation time. The plasmon energy is related to these parameters via

$$E_P = \hbar\left(\frac{1}{\varepsilon_{opt}\varepsilon_0\rho\tau}\right)^{1/2} = \hbar\left(\frac{Ne^2}{\varepsilon_{opt}\varepsilon_0 m^*}\right)^{1/2}, \tag{2}$$

where $\varepsilon_{opt} = C + A_{pole}/E_{pole}^2$, N is the hole concentration, and m^* the carrier's effective mass. Strictly speaking, we should include two Drude terms (one for heavy holes and one for light holes), but we obtain an excellent fit with a single term representing mainly the dominating heavy-hole contribution. Mathematically, the sum of two Drude terms with plasmon energies E_P^{hh} and E_P^{lh} reduces to a single Drude term with plasmon energy $E_P = [(E_P^{hh})^2 + (E_P^{lh})^2]^{1/2}$ if the relaxation time is the same for both bands. The third term in Eq. (1) corresponds to either two or three Gaussian oscillators ($m = 2, 3$). It describes the optical transitions between SO, LH, and HH bands. The fourth term describes the dispersion caused by absorption due to interband transitions outside the spectral range. The pole energy E_{pole} was maintained fixed at 2 eV. All adjustable parameters in the model, including the thicknesses of surface layer and the film layer, are fitted using a proprietary Marquardt-Levenberg algorithm provided by the ellipsometer's manufacturer. To verify that the model dielectric function is a realistic representation of the true dielectric function of the material, so-called point-by-point fits were performed.[6] These nonparametric fits adjust the value of the dielectric constant at each wavelength to fit the ellipsometric angles, without assuming any particular dispersion model. The nonparametric dielectric functions obtained for a $Ge_{0.98}Sn_{0.02}$ alloy and a Ge substrate from a point-by-point fit are shown in Fig. 2. The oscillator model in Eq. (1) is found to be in excellent agreement with this nonparametric dielectric function. This guarantees Kramers-Kronig consistency between the real and imaginary parts of the point-by-point dielectric function and confirms that three Gaussian oscillators are sufficient to capture the true line shape of the intervalence-band transitions.

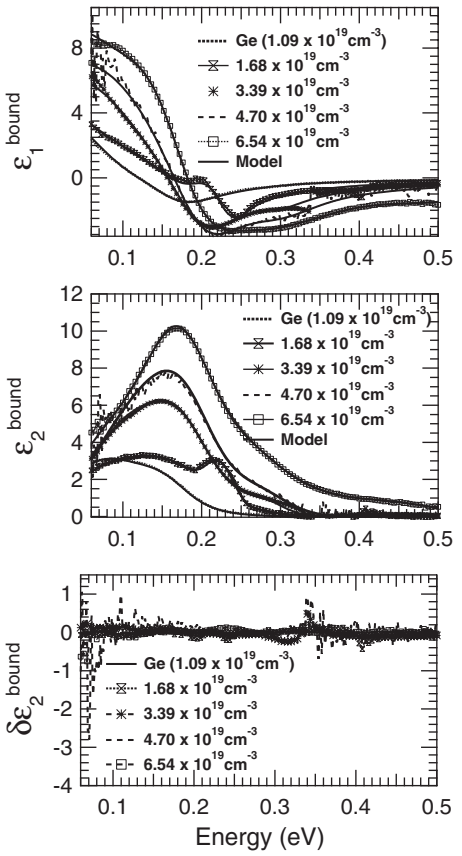

FIG. 4. Contribution from intervalence-band transitions to the real (a) and imaginary (b) parts of the nonparametric dielectric function of various *p*-doped $Ge_{0.98}Sn_{0.02}$ alloys and a *p*-doped Ge. The solid line represents the oscillator model described by the third term in Eq. (1). (c) The difference between the nonparametric and modeled dielectric function.

B. Infrared dielectric function

The IR dielectric function for *p*-doped $Ge_{0.98}Sn_{0.02}$ alloys is shown in Figs. 3(a) and 3(b). Besides the typical free-carrier response, additional features are observed corresponding to intervalence-band transitions between LH-HH, SO-HH, and SO-LH, respectively. The excellent agreement between parametric and nonparametric dielectric functions described in the previous section does not necessarily imply that the model in Eq. (1) provides an equally accurate description of the *individual* free-carrier and intervalence-band contributions to the dielectric function. To address this issue, we show in Fig. 4 the contribution of the intervalence-band transitions to the dielectric function after subtracting the model Drude contribution from the nonparametric dielectric function. The agreement between the intervalence-band contribution from the model and the intervalence-band contribution from the nonparametric dielectric function is excellent. The differences between the nonparametric dielectric function and modeled dielectric function $\delta\varepsilon_2$ are shown in Fig. 4(c). Furthermore, this also confirms that the free-carrier response can be described accurately by a single Drude term. Thus, the line shapes and the parameters deduced from the optical dispersion model can be used to gain quantitative

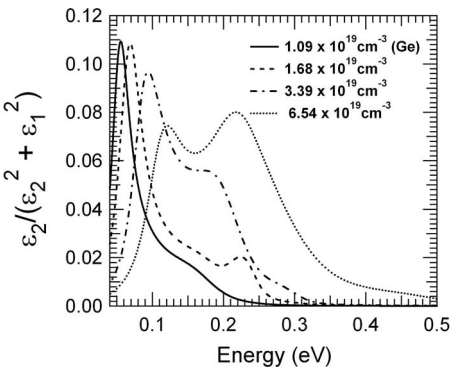

FIG. 5. Energy-loss spectra for various heavily doped *p*-type $Ge_{0.98}Sn_{0.02}$ alloys and a *p*-doped Ge. The solid line represents the *p*-doped Ge substrate.

understanding of the free-carrier response as well as the intervalence-band transitions. As a cautionary note, we emphasize that it is not always possible or easy to separate the free-carrier contribution from intervalence-band transitions in a unique manner. For example, Singley *et al.*[25] discussed the case of $Ga_{1-x}Mn_xAs$ alloys, in which the broadening parameter associated with the Drude term is $\sim$5000 cm^{-1}, more than one order of magnitude larger than ours, which range from 144 to 263 cm^{-1}. In this limit of large broadening, it is not possible to uniquely separate the intraband free-carrier contribution from the intervalence-band contribution without additional assumptions or insights. In our case, by contrast, the two contributions can be easily distinguished, as

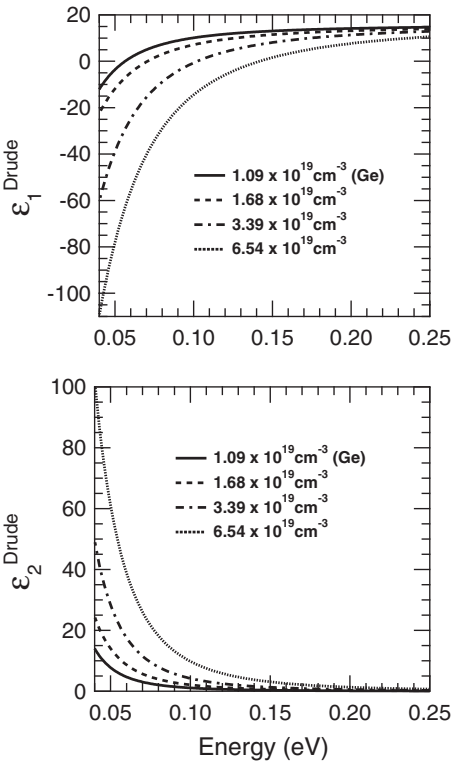

FIG. 6. Free-carrier response contribution to the real (a) and imaginary (b) parts of dielectric function of *p*-doped $Ge_{0.98}Sn_{0.02}$ alloys and a *p*-doped Ge.

TABLE I. Transport parameters and plasmon energies for $Ge_{0.98}Sn_{0.02}$ alloys with various doping concentrations. N and μ are obtained by assuming an effective hole mass of $0.27m_e$.

Sample	ρ (Ω cm)	τ fs(cm^{-1})	ε_{opt}	E_P (eV)	N (10^{19} cm^{-3})	μ (cm^2 V^{-1} s^{-1})
Ge1	0.0027	32.3 (164)	15.4	0.060	1.09	210
Ge2	0.0014	36.8 (144)	13.8	0.081	1.80	240
98A	0.0023	25.3 (210)	15.1	0.075	1.68	165
95B	0.0015	27.6 (192)	15.2	0.087	2.28	180
90A	0.0011	25.2 (210)	15.5	0.105	3.39	164
98C	0.00077	26.4 (201)	15.2	0.125	4.70	172
91C	0.00073	20.2 (263)	15.7	0.145	6.54	132

discussed above. The clear separation between the two contributions can also be seen by considering the loss function

$$\mathrm{Im}\left(\frac{1}{\varepsilon_1 + i\varepsilon_2}\right) = \frac{\varepsilon_2}{\varepsilon_1^2 + \varepsilon_2^2}. \quad (3)$$

Figure 5 shows the energy-loss spectrum computed from Eq. (3) for the doped alloys. Two peaks are observed, which correspond to the two main contributions (intraband and intervalence-band transitions) to the dielectric function.

IV. RESULTS AND DISCUSSION

A. Free carrier response

The infrared dielectric function corresponding to the free-carrier response of $Ge_{0.98}Sn_{0.02}$ alloys for various doping concentrations is shown in Fig. 6. The Drude term in Eq. (1) gives the electrical resistivity and the carrier relaxation time. The plasmon energy for $Ge_{0.98}Sn_{0.02}$ alloys shifts to higher energy with doping concentration, as expected from Eq. (2). Table I shows the plasmon energies and all the parameters obtained from the Drude model. Since the ellipsometric measurements depend on the carrier concentration via the ratio N/m^*, the doping level can only be obtained if independent measurements of the effective mass are available. In Table I we have simply assumed that the effective mass of the alloy is $m^*=0.27m_e$, the same as that of Ge.[11] Based on this assumption, Fig. 7 shows the electrical resistivity of $Ge_{0.98}Sn_{0.02}$ alloys as a function of doping concentration. The solid line shows a fit to Ge resistivity data obtained from electrical measurements. Notice that the resistivity of Ge determined by ellipsometry (squares) agrees well with the electrical measurements.[26]

The agreement of the alloy and the Ge data over one order of magnitude in doping concentrations strongly suggests that the effective masses are indeed very similar. However, we cannot rule out the validity of the band antricrossing model based on these results, for a modest increase in the hole effective mass in $Ge_{0.98}Sn_{0.02}$ relative to Ge would be virtually undetectable within the error of our measurements.

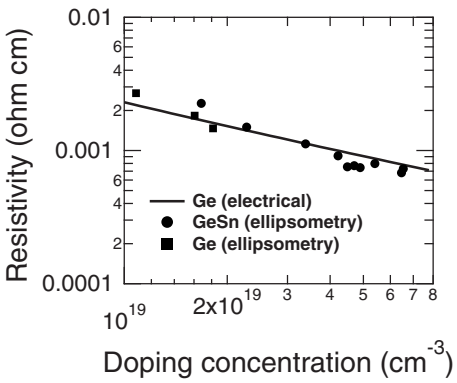

FIG. 7. Electrical resistivity of p-type $Ge_{0.98}Sn_{0.02}$ alloys as a function of doping concentration. The solid line represents the resistivity of doped Ge determined by Hall measurements. The squares represent the resistivity of doped Ge obtained by ellipsometry.

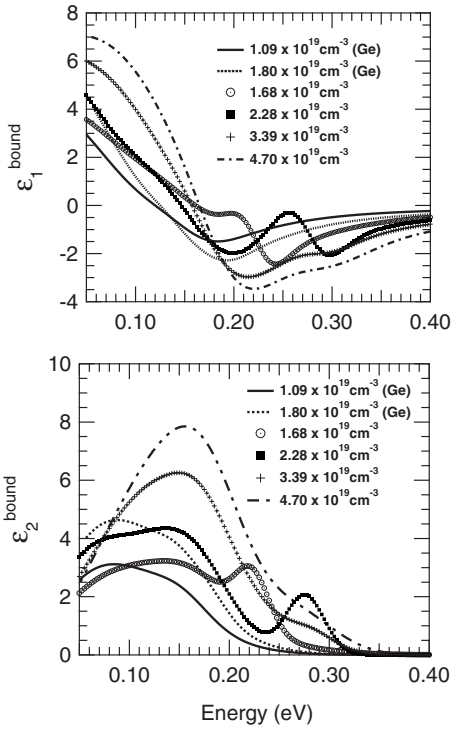

FIG. 8. Contribution from intervalence-band transitions to the real (a) and imaginary (b) parts of dielectric function of various p-doped $Ge_{0.98}Sn_{0.02}$ alloys and a p-doped Ge. The solid line and the dotted line represent the two p-doped Ge substrates.

TABLE II. Intervalence-band transitions' parameters for $Ge_{1-y}Sn_y$ alloys with various doping concentrations. Three transitions are observed in GeSn alloys, which correspond to LH-HH, SO-LH, and SO-HH transitions.

Sample	y (%)	$\varepsilon_{\parallel}$ (%)	E_A (eV)	A_B	E_B (eV)	Γ_B (eV)	A_C	E_C (eV)	Γ_C (eV)
Ge1	0	0	0.083	0.63	0.154	0.063	0.63	0.154	0.063
Ge2	0	0	0.087	1.02	0.161	0.067	1.02	0.161	0.067
98A	1.7	0.13	0.100	0.88	0.166	0.081	1.84	0.223	0.040
95B	2.0	0.15	0.074	2.77	0.161	0.091	2.01	0.276	0.046
90A	1.5	0.15	0.131	0.98	0.173	0.063	0.45	0.283	0.051
98C	1.6	0.13	0.121	3.77	0.179	0.090	1.34	0.268	0.089
91C	1.2	0.15	0.155	3.48	0.170	0.078	0.65	0.441	0.149

B. Intervalence-band transitions

The real and imaginary parts of dielectric function corresponding to the intervalence-band transitions are shown in Fig. 8. For pure Ge, we observe two main features, which are satisfactorily fit with two Gaussian oscillators, with parameters given in Table II. The lower-energy component near 0.10 eV can be associated with LH-HH transitions, whereas the shoulder at 0.15 eV energy is related to both SO-HH and SO-LH transitions. These transitions are not clearly resolved in the dielectric function of the two doped Ge samples, in part due to the fact that the light and heavy holes are degenerate at the center of the Brillouin zone. The line shape of the intervalence-band dielectric function observed here is very similar to that reported by Humlíček[21,22] The intervalence-band transitions in p-doped $Ge_{0.98}Sn_{0.02}$ look markedly different. These results confirm that the spectroscopy of intervalence-band transitions provides a much more sensitive probe of the valence-band structure of the alloys than the free-carrier response. For the lowest doping concentrations, we see a broad structure below 0.20 eV that roughly agrees with the observed line shape of the two pure Ge samples with similar doping concentrations; but in addition there is a relatively sharp feature above 0.20 eV whose energy increases as the doping level is increased. A fit of this complex structure requires three Gaussian oscillators, and the corresponding parameters are given in Table II. It is tempting to assign the new features seen in the alloy dielectric function to the modification of the valence-band dispersion relations predicted by the band anticrossing model, but a detailed calculation of the intersubband absorption within this model would be needed to make the connection to experiment. A possible complication of such a study is the observation that intervalence-band absorption is strongly dependent on strain.[27] Thus, the residual strain in our films may play an unexpectedly significant role and will have to be included in any realistic simulation.

V. CONCLUSIONS

Infrared optical studies using spectroscopic ellipsometry have been carried out on p-doped $Ge_{0.98}Sn_{0.02}$ alloys ($p > 10^{19}$ cm^{-3}). The transport properties deduced from the optical experiments are very similar to those of pure Ge, but differences with Ge are seen in the line shape of intersubband transitions. These differences may represent an important tool to assess the validity of different models of the electronic structure of $Ge_{1-y}Sn_y$ alloys. In particular, the band anticrossing model of Alberi *et al.* makes specific predictions for the band dispersions that could be compared directly with our experiments. We hope that the results presented here will stimulate a theoretical effort to calculate intervalence-band transitions in $Ge_{1-y}Sn_y$ alloys.

The similarity in the transport properties of p-type $Ge_{1-y}Sn_y$ alloys and pure Ge bodes well for the fabrication of $Ge_{1-y}Sn_y$ devices. A similar result was found for the n-type material.[11] Work to prepare and characterize p-n junctions is currently in progress.

ACKNOWLEDGMENTS

This work was supported by the U.S. Air Force under Contract No. DOD AFOSR FA9550-06-01-0442 (MURI program) and by the U.S. Department of Energy under Grant No. DE-FG36-08GO18003.

[1] R. A. Soref, J. Kouvetakis, J. Tolle, J. Menéndez, and V. R. D'Costa, J. Mater. Res. **22**, 3281 (2007).
[2] R. Roucka, J. Xie, J. Kouvetakis, J. Mathews, V. D. Costa, J. Menendez, J. Tolle, and S. Q. Yu, J. Vac. Sci. Technol. B **26**, 1952 (2008).
[3] G. He and H. A. Atwater, Phys. Rev. Lett. **79**, 1937 (1997).
[4] D. W. Jenkins and J. D. Dow, Phys. Rev. B **36**, 7994 (1987).
[5] K. A. Mäder, A. Baldereschi, and H. von Kanel, Solid State Commun. **69**, 1123 (1989).
[6] V. R. D'Costa, C. S. Cook, A. G. Birdwell, C. L. Littler, M. Canonico, S. Zollner, J. Kouvetakis, and J. Menendez, Phys. Rev. B **73**, 125207 (2006).
[7] H. Perez Ladron de Guevara, A. G. Rodriguez, H. Navarro-Contreras, and M. A. Vidal, Appl. Phys. Lett. **91**, 161909

(2007).
[8] K. Alberi, J. Blacksberg, L. D. Bell, S. Nikzad, K. M. Yu, O. D. Dubon, and W. Walukiewicz, Phys. Rev. B **77**, 073202 (2008).
[9] W.-J. Yin, X.-G. Gong, and S.-H. Wei, Phys. Rev. B **78**, 161203 (2008).
[10] A. V. G. Chizmeshya, C. Ritter, J. Tolle, C. Cook, J. Menendez, and J. Kouvetakis, Chem. Mater. **18**, 6266 (2006).
[11] V. R. D'Costa, J. Tolle, J. Xie, J. Menéndez, and J. Kouvetakis, in *Transport Properties of Doped GeSn Alloys* (AIP, Rio de Janeiro, 2008).
[12] P. Y. Yu and M. Cardona, *Fundamentals of Semiconductors: Physics and Materials Properties* (Springer-Verlag, Berlin, 1996).
[13] J. D. Sau and M. L. Cohen, Phys. Rev. B **75**, 045208 (2007).
[14] M. V. Fischetti and S. E. Laux, J. Appl. Phys. **80**, 2234 (1996).
[15] E. T. Thomas, D. M. Aaron, and A. W. John, *Measurement of Silicon Doping Profiles Using Infrared Ellipsometry Combined with Anodic Oxidation Sectioning* (AIP, Melville, NY, 1998), p. 221.
[16] T. E. Tiwald, D. W. Thompson, J. A. Woollam, W. Paulson, and R. Hance, Thin Solid Films **313-314**, 661 (1998).
[17] H. B. Briggs and R. C. Fletcher, Phys. Rev. **87**, 1130 (1952).
[18] W. Kaiser, R. J. Collins, and H. Y. Fan, Phys. Rev. **91**, 1380 (1953).
[19] A. H. Kahn, Phys. Rev. **97**, 1647 (1955).
[20] E. O. Kane, J. Phys. Chem. Solids **1**, 82 (1956).
[21] J. Humlíček, Thin Solid Films **313-314**, 656 (1998).
[22] J. Humliček and V. Křapek, *Infrared Response of Heavily Doped p-type Si and SiGe Alloys from Ellipsometric Measurements* (AIP, Melville, NY, 2005), p. 113.
[23] C. Chen, J. Liu, B. Yu, and Q. Dai, Microelectron. J. **38**, 392 (2007).
[24] C. F. Bohren and D. R. Huffman, *Absorption and Scattering of Light by Small Particles* (Wiley-Interscience, New York, 1983).
[25] E. J. Singley, R. Kawakami, D. D. Awschalom, and D. N. Basov, Phys. Rev. Lett. **89**, 097203 (2002).
[26] D. B. Cuttris, Bell Syst. Tech. J. **40**, 509 (1961).
[27] I. Balslev, Phys. Rev. **177**, 1173 (1969).